analytical chemistry

ARTICLE

pubs.acs.org/ac

Optimizing Label-Free DNA Electrical Detection on Graphene Platform

Emilie Dubuisson, Zhiyong Yang, and Kian Ping Loh*

Department of Chemistry, National University of Singapore, 3 Science Drive 3, Singapore 117543

Supporting Information

ABSTRACT: The anodized epitaxial graphene (EG) electrode demonstrates a high level of performance for electrochemical impedance as well as differential pulse voltammetry detection of immobilized DNA and free DNA, respectively, at solid−liquid interfaces. On the anodized EG surface, because of the presence of oxygen functionalities as well as π conjugated domains, the anchoring of the DNA probe can be achieved by either covalent grafting or noncovalent $\pi-\pi$ stacking readily. The effect of different binding modes on the sensitivity of the impedimetric sensing was investigated. Equivalent circuit modeling shows that the sensitivity of EG to DNA hybridization is controlled by changes in the resistance of the molecular layer as well as the space charge layer. The linear dynamic detection range of EG for DNA oligonucleotides is in the range of 5.0×10^{-14} to 1×10^{-6} M. In addition, with the use of differential pulse voltammetry, single stranded DNA, fully complimentary DNA, as well as single nucleotide polymorphisms can be differentiated on anodized EG by monitoring the oxidation signals of individual nucleotide bases.

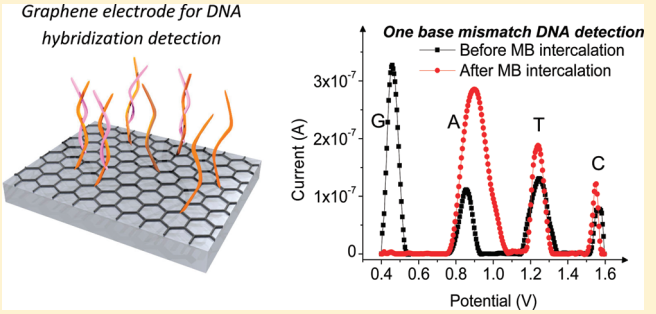

Graphene, a single layer of carbon atoms in a closely packed honeycomb two-dimensional structure, is a new kind of nanostructured carbon material.[1] Because of its novel properties,[2,3] the use of graphene in optoelectronic devices,[4] Li-ion batteries,[5] optical applications,[6] and electrochemical sensors[7,8] is believed to give enhanced performance. Oxygenated graphene (graphene oxide) prepared by the acid exfoliation of graphite or electrochemical anodization can undergo a broad class of organic/functionalization reactions owing to the presence of carboxylic and hydroxyl groups acting as linkers. The combination of the aromatic scaffold as well as oxygenated functional groups allows the graphene oxide platform to be readily functionalized via covalent coupling reactions or noncovalent $\pi-\pi$ stacking.[9−11]

To date, various fabrication methods for different forms of graphene have been explored, such as reduced graphene oxide,[12] chemical vapor deposited graphene,[13−15] chemically exfoliated graphene,[16,17] and epitaxial graphene (EG) grown on silicon carbide (SiC).[18] Among these techniques, the use of SiC substrates has been demonstrated to be a reliable way to provide high-quality crystalline graphene films[18] and the presence of an insulating substrate (SiC) renders it amenable to mass-scale fabrication of electronic devices and electrode applications. Being a single layer atomic sheet, graphene is by nature highly sensitive to changes in its electromagnetic environment and should exhibit unique advantages as electrodes for the electrochemical sensing of biomolecules. Our group has previously investigated the effect of edge plane defect on the electrochemical and sensing activities of EG and has demonstrated that anodized EG, consisting of oxygen-related defects, is a superior platform for voltammetric sensing as opposed to pristine graphene.[19]

Electrochemical impedance spectroscopy (EIS) is a noninvasive technique that probes the change in charge transfer resistance at the electrode following bioaffinity events. This technique is especially useful in bioanalytics for label-free detection since it bypasses the need to modify the biomolecules with labels. DNA sensors performance based on EIS strongly depends on the physical characteristics of the immobilized DNA probe layer and on the electrode surface properties. Stable and reproducible immobilization of biological macromolecules on the electrode surface is an important criteria for the sensitive and robust sensing of biological events.

In this paper, we evaluate the sensitivity and chemical robustness of anodized EG platform for biosensing at the solution−electrode interface. The frequency-dependent impedimetric response of DNA-modified anodized EG surfaces to complementary and non cDNA sequences is investigated. Two methods of biofunctionalization based on covalent grafting (Figure 1a) and non covalent $\pi-\pi$ stacking (Figure 1b) were investigated with a view toward identifying the method which can produce a larger signal-to-noise change in bioaffinity events. This impedimetric platform based on EG was systematically compared with highly ordered pyrolytic graphite (HOPG). In addition, the ability of anodized EG for the direct voltammetric sensing of single base polymorphism was demonstrated successfully.

Received: September 15, 2010
Accepted: February 12, 2011
Published: March 03, 2011

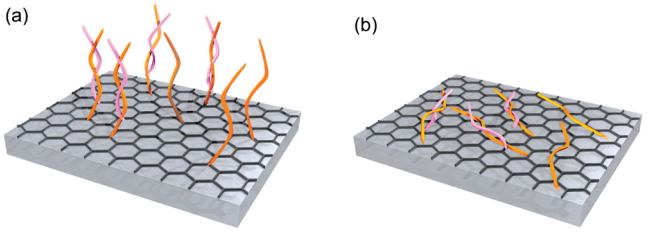

Figure 1. Schematic representations of the different strategies for DNA-probes immobilization onto EG surface (orange DNA fragments) and their hybridization with cDNA-target (pink DNA fragments). (a) DNA-probes are covalently grafted. (b) DNA molecules are attached to the anodized EG surface by $\pi-\pi$ stacking.

EXPERIMENTAL DETAILS

Chemical Reagents. Phosphate buffered saline (PBS 10×, 0.14 M NaCl + 2.7 mM KCl + 10 mM Na_3PO_4 + 1.76 mM K_3PO_4, pH 7.4) was obtained by first Base, Singapore. 1-Ethyl-3-(3-dimethylaminopropyl)carbodiimide hydrochloride (EDC) and *N*-hydroxysuccinimide (NHS) were purchased from Sigma and used directly without further purification.

The 30 mer oligonucleotides were synthesized by first Base. The probe DNA is modified at the 5′-end with an alkylamino modifier (NH_2-ssDNA probes, sequence: NH_2-C_{12}-5′-GCA CCT GAC TCC TGT GGA GAA GTC TGC CGT-3′). The DNA-targets contain either fully complementary sequence to the probe DNA (5′-ACG GCA GAC TTC TCC ACA GGA GTC AGG TGC-3′) or one-base mismatch to the probe DNA (5′-ACG GCA GAA TTC TCC ACA GGA GTC AGG TGC- 3′). The fully noncomplementary target has the following sequence: 5′-GTA CAT CTA GCA CGT GGC TAG AGT TAC CAT-3′. All the DNA fragments were diluted in PBS 1× by careful serial dilution. The DNA solutions were stocked at −20 °C to avoid denaturation. Highly ordered pyrolytic graphite was obtained by SPI Supplies (Singapore).

Preparation of Epitaxial Graphene (EG). Silicon carbide substrates used for EG growth were cut from nitrogen doped, on-axis oriented, double side polished, research grade, (0001) face (Si-terminated) 6H-SiC wafers, purchased from Cree. The substrate was introduced into a UHV chamber (10^{-10} Torr) equipped with reflection high energy electron diffraction (RHEED, Oxford Applied Research). Parameters for RHEED pattern recording include an incident electron beam energy of 28.3 keV and filament current of 2.40−2.45 A. An infrared pyrometer allowed the measurement of substrate temperature during silicon dosing and annealing. After degassing, the sample was resistively heated to 850 °C, following which a current of 18.5 A was applied to the Si evaporator to evaporate Si on the sample for 3 min. The sample was then cooled down. A series of annealing steps followed subjected to a maximum temperature of 1250 °C, until a $(6\sqrt{3} \times 6\sqrt{3})$-R30° RHEED pattern was observed.

DNA Probes Immobilization and Targets Hybridization. For the immobilization of the probe DNA (NH_2-ssDNA) onto the carboxyl group of anodized EG, the surface of the working electrode was activated with EDC (0.2 M) and NHS (0.5 M) for 1 h. After a rinse with pure water, the DNA solution was added and the solution was incubated overnight for grafting. At the end of the incubation, the electrode was rinsed thoroughly with the immobilization buffer and exposed to 100 μL of ssDNA targets solution for hybridization. After 40 min at 42 °C, the electrode was rinsed with the hybridization buffer. The same process was used for the target with one-base mismatch or noncomplementary target.

Intercalation of Methylene Blue. A solution of Methylene Blue (MB) 1 mM + NaCl 50 mM was prepared. To intercalate MB into the DNA duplex structure, 0.1 mL of this solution was added in the electrochemical cell. After 5 min at 60 °C and cooling until 25 °C, differential pulse voltammetry (DPV) measurements were performed.

Electrochemical System. A three-electrode system was used for anodization, EIS, and DPV measurements. The EG is used as a working electrode, and an Ag/AgCl (in saturated KCl) electrode and a Pt wire were used as the reference and auxiliary electrodes, respectively. The electrochemical measurements were carried out using a Autolab PGSTAT30 digital potentiostat/galvanostat with a FRA2 module. All the measurements were carried out in a polytetrafluoroethylene (PTFE) house (V = 5 mL). The working electrode was clamped tightly at the base of the PTFE housing with a 2 mm diameter O-ring. The exposed surface area of the working electrode was 0.0314 cm^2. See a detailed representation in the Supporting Information (Figure S1).

Impedance spectra were measured at −0.4 V from 100 kHz down to 0.1 Hz with an ac amplitude of 10 mV. The application of a negative potential is appropriate to prevent the oxidation of the oligonucleotides. Impedance measurements were obtained in a standard hybridization buffer solution consisting of PBS (14 mM NaCl, 0.27 mM KCl, 1 mM Na_3PO_4 and 0.176 mM K_3PO_4), without any redox couple added. Redox-free impedance spectroscopy has been reported frequently for the investigation of biointerfaces such as protein adsorption studies,[20−22] DNA sensing[23−25] and biointeraction between materials and tissues.[26] The charge transfer resistance in this case arises from ionic transport in the PBS electrolyte across a resistive biomolecular layer on the graphene electrode. The migration of these ionic species through the biomolecular layers (ssDNA or dsDNA) is affected by the interfacial charge distribution during biorecognition events.

DPV measurements were conducted based on the following parameters: 60 s accumulation time at 0.2 V, 50 ms modulation time, 0.5 s interval time, 25 mV modulation amplitude, and 5 mV step. The raw data were treated with the Savitzky and Golay filter of the Fra software (Eco Chemie, The Netherlands), followed by the moving average baseline correction with a peak width of 0.005.

RESULTS AND DISCUSSION

Anodization of Epitaxial Graphene. Because of the two-dimensional nature of graphene sheets, the edge regions play an important role in the electrochemical activity.[27−30] Heterogeneous electron transfer has been reported to take place on the edges of the graphene, while heterogeneous electron transfer from the plane of a graphene sheet is almost nil.[31] Previous reports indicated that the appearance of edge plane defects on the HOPG basal plane induced an increase in the electron transfer rate constant.[32] Such defect sites are important in the application of EG as electrodes for sensing. Thus, with the aim of facilitating fast electron transfer kinetics, we anodized the EG surface adequately to create edge planes,[19] the outcome of which would be the fracturing of the lattice and formation of edge plane defects.[33] The anodization creates ionizable oxygenated groups

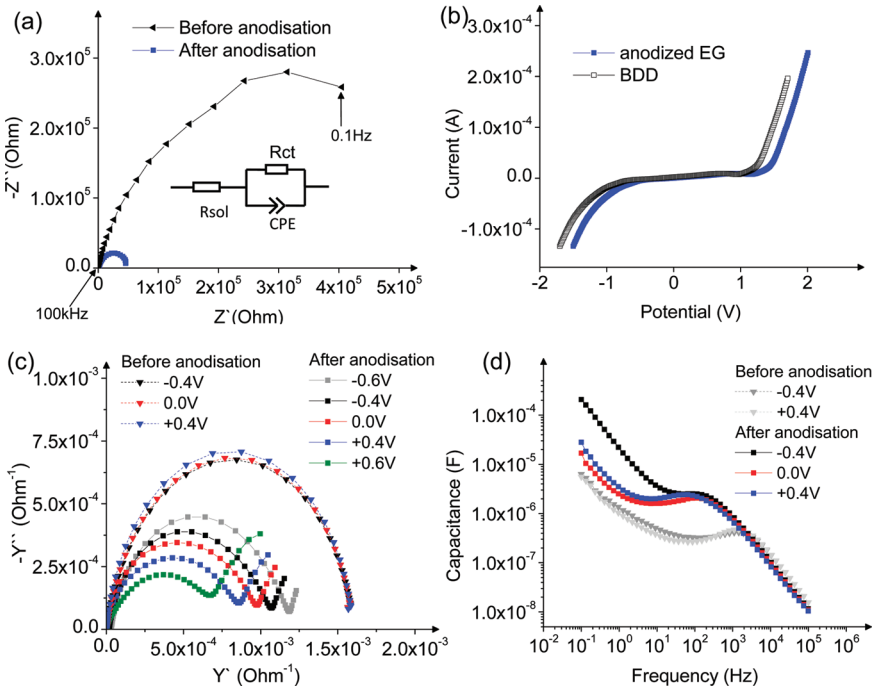

Figure 2. (a) Nyquist plot of EG electrode before (black solid triangle) and after (blue solid square) anodization. The inset is the equivalent circuit. (b) Electrochemical window of anodized EG (blue solid square) and BDD (black open square) electrodes at 50 mV s^{-1} in 1 M KCl. (c) Admittance plot before (dashed line) and after anodization (full line) of epitaxial graphene electrode under different potentials vs Ag/AgCl. (d) Corresponding capacitance vs frequency plot.

which can act as tethering groups for biomolecules and allow easy biofunctionalization of the electrode.

Electrochemical impedance spectrosopy (EIS) was used to characterize the influence of anodization on the electrochemical properties of the electrode. As shown in Figure 2a, after anodization of epitaxial graphene at 2.0 V vs Ag/AgCl for 300 s in a phosphate buffered saline solution (PBS 10×), the impedance modulus experienced a substantial decrease. Since the electrolyte resistance is constant, the charge transfer resistance arises from ionic transport across the electrode. By fitting experimental data with its equivalent circuit model (see inset in Figure 2a), the dramatic change in the radius of the semicircle in the Nyquist plot after anodization indicates a reduction in the charge transfer resistance by almost 5 orders of magnitude. This can be rationalized by the creation of edge plane defects on the anodized graphene, these edge planes protruding from the surface allow lateral charge transfer to occur "out of plane" and enhance the electrochemical activity dramatically.

In addition, the 2 V wide electrochemical potential window of anodized EG (Figure 2b) is comparable to boron-doped diamond (BDD) electrode, which is well-known for its chemical inertness.[34] A wide electrochemical potential window is necessary for observing well-resolved voltammetric peaks for DNA bases, as the latter have high oxidation potentials that lie outside the electrochemical potential windows of most conventional electrodes.

Both graphene and graphene oxide (GO) are chemically tunable and interconvertible to some extent.[35,36] For example, the EG electrode can be electrochemically oxidized (anodized) and that produces a metallic-to-semiconductor transition in the electrical properties, which is essential for developing a sensitive sensor. In view of the fact that anodization-induced changes in impedance are visible at high frequencies, an alternative representation was used to emphasize these changes: the complex admittance plot,[37] $Y' = \mathrm{Re}(1/Z) = (Z'/|Z|^2)$, $Y' = \mathrm{Im}(1/Z) = -Z'/|Z|^2$ as shown Figure 2c. In the admittance plot, high frequencies are on the right side and low frequencies on the left side (as opposed to the Nyquist plot). Changes at the small frequencies are usually dominated by resistive elements and those at high frequencies by the capacitive element, such as the space-charge layer, thus any changes in the latter can be highlighted clearly in an admittance plot. Figure 2c reveals that before anodization, at high frequencies, the admittance plot is independent of the applied potential. After EG anodization, the admittance plot shows strong dispersion with the applied voltages. This is characteristic of semiconductor behavior and indicates that a space-charge layer was created, dominating the admittance response.

Detailed analysis of complex capacitance as a function of frequency was also investigated. Complex capacitance can be expressed as[38]

$$Z(\omega) = \frac{1}{j\omega C(\omega)} \quad (1)$$

and

$$C(\omega) = C'(\omega) - jC''(\omega) \quad (2)$$

Manipulation of eqs 1 and 2 leads to

$$C'(\omega) = \frac{-Z''(\omega)}{\omega|Z(\omega)|^2} \quad (3)$$

and

$$C''(\omega) = \frac{Z'(\omega)}{\omega|Z(\omega)|^2} \quad (4)$$

dx.doi.org/10.1021/ac102431d |*Anal. Chem.* 2011, 83, 2452–2460

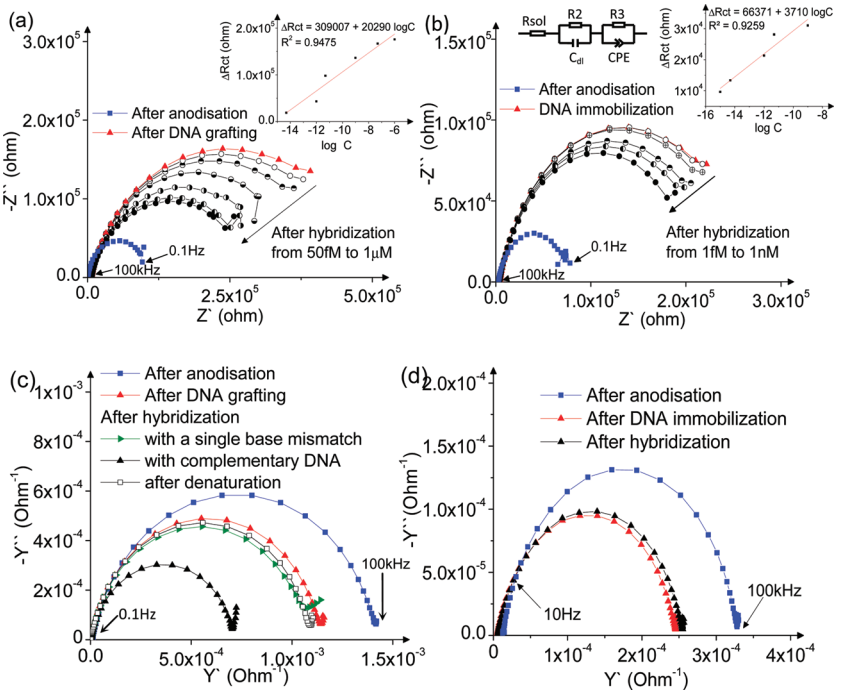

Figure 3. Nyquist plot before (blue solid square) and after (red solid triangle) DNA-probe immobilization by (a) covalent grafting and (b) $\pi-\pi$ stacking; after incubating the electrodes in a hybridization buffer containing different concentrations of DNA-target for 40 min at 42 °C: (a) 50 fM, 1 pM, 50 pM, 1 nM, 50 nM, and 1 μM and (b) 1 fM, 50 fM, 1 pM, 50 pM, and 1 nM. Inset: Plot of ΔR_{ct} against the concentration of DNA-target and equivalent circuit modeling. Corresponding admittance plot for (c) covalent grafting or (d) $\pi-\pi$ stacking plot before (blue solid square) and after DNA-probe immobilization (red solid triangle), after incubation in the presence of a single base mismatch DNA solution (solid green triangle) or cDNA-target (solid black curve) 1 nM and after denaturation (open square).

where C' and C'' are the real and imaginary part of the capacitance, respectively, and expressed in terms of real, imaginary, and total impedance. Figure 2d represents the modulus of the total complex capacitance as a function of frequency. Before anodization, no significant change was observed under different applied potential, confirming the previous results obtained by admittance. After anodization, a strong increase in the total capacitance is observed for frequencies below 10 kHz, due to the creation of a space charge layer. Thus, at −0.4 V vs Ag/AgCl, total capacitance values, before and after anodization, are 2.23×10^{-6} and 2.21×10^{-5} F, respectively. Moreover, after anodization, the capacitance disperses with applied potential. For n-type semiconductor, the space-charge region is expected to be in the accumulation regime at the negative potentials, which lead to higher space-charge capacitance. Thus, anodized EG presents n-type semiconductor characteristics.

In the following impedimetric studies, anodized EG samples with space charge layer will be used in the DNA sensing experiments.

DNA Detection by Electrochemical Impedance Spectroscopy. EIS was carried out to study the changes induced by DNA probes immobilized by covalent grafting or by $\pi-\pi$ stacking on the anodized EG surface. In EIS, the diameter of the semicircle is indicative of the charge transfer resistance, R_{ct}. Its value varies depending on the charge transfer resistance of the biomolecular layers that are covalently grafted on the electrode surface. As shown in Figure 3a,b, after DNA-immobilization by covalent grafting or by $\pi-\pi$ stacking, an increase in the charge transfer resistance of ~315% and 175% was observed, respectively. This proves the success of DNA immobilization and also indicates a higher density of DNA coverage for the covalently grafted DNA probe compared to the $\pi-\pi$ stacked DNA probes.

After hybridization with complementary target, EIS measurements show that the charge transfer resistance decreases with increasing concentrations of cDNA-target for both immobilizations (Figure 3a,b). It is well-known that double stranded DNA (i.e., after hybridization with a complementary sequence) is more conductive than single-stranded DNA.[39−41] Moreover, single-stranded DNA fragments are flexible and can lie on the electrode surface, thus blocking effective electron transfer. However, upon DNA hybridization, effective electron transfer increases as the hybridized cDNA strands now become "rigid" and "stand up" on the electrode surface, resulting in a decrease in the charge transfer resistance. The differences in the charge-transfer resistance ΔR_{ct} between single stranded DNA (before hybridization) and duplex DNA (after hybridization) indicates a structural rearrangement from single stranded DNA to duplex. As shown in the inset of Figure 3a,b, the calibration curve indicates that the values of ΔR_{ct} ($\Delta R_{ct} = R_{ct,dsDNA} - R_{ct,ssDNA}$) were linear with the logarithmic concentration of DNA. A good linearity range between 5×10^{-14} and 1×10^{-6} M and 5×10^{-14} to 1×10^{-9} M was established for electrode biofunctionalized by covalent grafting and $\pi-\pi$ stacking, respectively. The relationship between the sensor variable (e.g., R_{ct}) and the target concentration should be linear if it follows the Langmuir adsorption kinetics as R_{ct} is related to the electrode surface coverage of the target molecule. However, in our experiment, a logarithmic relationship was obtained up to the saturation point. The probe-target binging is likely to be heterogeneous due to a random distribution of the probes on the electrode surfaces. Therefore, the typical Langmuir isotherm cannot be applied here and the Temkin isotherm is a better model to explain the observed results, in which case a logarithmic relationship was observed.[42−44]

dx.doi.org/10.1021/ac102431d |*Anal. Chem.* 2011, 83, 2452–2460

The dynamic range, corresponding to the relationship between the sensor variable and DNA concentration, depends strongly on the electrode surface properties as well as the method of DNA-probe immobilization. A wide dynamic range can be obtained for highly sensitive impedimetric sensors.[42,45,46] The EG sensor prepared with covalently grafted DNA probes presents a high dynamic range with a low detection limit of 2×10^{-14} M defined at 3σ (where σ is the standard deviation of a blank solution) and an interelectrode reproducibility of 7% for 1 nM. For DNA-probe immobilization by $\pi-\pi$ stacking, the DNA-probes seem to be fully hybridized in the presence of 1 nM DNA-target solution whereas a 1000× higher concentration (1 μM) target DNA is needed for a covalently grafted DNA probe. In the case of DNA probes immobilized by $\pi-\pi$ stacking, an increase in the impedance can be detected (data not shown) at a concentration of target DNA > 50 nM, this may be due to the random adsorption of excess DNA on the surface, introducing disorder into the film and giving rise to a higher ΔR_{ct}. In fact, circular dichroism results show that $\pi-\pi$ stacking of single-stranded DNA on graphene lead to unfolding of the DNA intrinsic structure, and this may have a negative effect on duplex formation with DNA-target molecules.[47]

One question is whether anodized EG presents any advantages compared to anodized highly ordered pyrolytic graphite (HOPG). To address this question, we compared the direct impedimetric DNA sensing on anodized HOPG and EG. DNA-probes were covalently grafted onto anodized HOPG using the same procedure for anodized EG. While significant changes in the Nyquist plot induced by DNA hybridization can be detected with DNA-target concentration as low as 50 pM using anodized HOPG, that for anodized EG is at least 3 orders of magnitude lower (50 fM) (see the Supporting Information, Figure S2a). Upon hybridization with 1 nM cDNA-target, there is a 16% change in the radius of the semicircle for anodized HOPG as compared to 31% for anodized EG.

Another issue is the presence of the layered structure in HOPG gives rise to higher capacitive noise due to nonfaradaic charging. The electrode capacitance value (C°) was obtained from cyclic voltammetry at 0.25 V versus Ag/AgCl in 1.0 M KCl (data not shown). The capacitance value for anodized HOPG is 1.2 mF/cm^2, which means it is about 400 times higher than that of anodized EG (2.73 μF/cm^2). Goh et al.[48] have shown that multilayer graphene nanoribbons exhibit larger capacitance than their few-layer and single-layer graphene counterparts. Although this is a significant advantage for energy storage devices, this is a potential drawback for impedimetric sensing which is based on the sensitive detection of small changes in the interfacial space-charge layer. Because of a larger background capacitance and more efficient screening of the space-charge layer for graphite, a small change in the interfacial capacitance or change in the surface charge cannot be as effectively detected by EIS using graphite compared to EG.

Admittance plots were also used to emphasize the hybridization-induced changes at high frequencies. Upon DNA immobilization and hybridization on anodized EG electrodes, an obvious change in admittance value was observed as shown in Figure 3c. A semicircle of the admittance plot decreases by 21% and 36%, respectively. Figure 3c,d shows the various control studies carried out to evaluate the repeatability and robustness of the sensor. In the evaluation experiment to determine the response to a single base mismatched target oligonucleotide (Figure 3c), there was no significant difference of admittance values before and after hybridization. This means that the probe oligonucleotide-modified electrode fabricated in this study specifically discriminated between matched and mismatched oligonucleotide sequences. Finally, by immersion of the hybridized electrode in 0.1 M NaOH for 240 s, the double stranded DNA was denatured and the electrical response of the denatured sample is almost identical to that of the starting surface (Figure 3c). These results testify to the robustness and regenerative characteristics of the DNA-EG impedimetric sensor.

Figure 3d shows the impedimetric response (admittance plot) of DNA-probes immobilized by $\pi-\pi$ stacking on anodized EG electrode. The semicircle of the admittance plot decreases by 25% upon probe immobilization. However upon hybridization, no significant change was observed.

The influence of bioaffinity events (DNA-probes immobilization and DNA hybridization) on the total capacitance was also investigated for covalent grafting (Figure S3a, Supporting Information) and $\pi-\pi$ stacking (Figure S3b, Supporting Information). Hybridization induces changes in capacitance from 0.1 Hz to 100 kHz for covalent grafting and only from 0.1 and 20 Hz for DNA-immobilized by $\pi-\pi$ stacking. This confirms the impedance and admittance results.

Because of the higher density of probe DNA, the dynamic range for detection is wider for DNA immobilized by covalent grafting compared to the $\pi-\pi$ adsorbed DNA. The dynamic range and sensitivity for DNA detection observed in our experiments with anodized EG are better than impedimetric assays based on graphite electrodes[49] but are comparable with electrochemical assays based on diamond nanowires,[50] multiwalled carbon nanotubes,[51,52] and CVD graphene transistor.[53]

Equivalent Circuit Modeling. There are different ways in which DNA hybridization can affect the electrical properties of the interface: changes in capacitance of the molecular layer or charge diffusion at the electrode surface or modification of the electronic properties of the space charge layer. To understand the electrical response and the hybridization-induced changes for both immobilization processes, the impedance data were analyzed using an equivalent circuit model (insert Figure 3b). The interface can be divided into three physical regions: the bulk solution, the molecular layer, and its associated double-layer and the space-charge layer in the graphene substrate. This electrical model consists of a resistance R_{sol} due to the ohmic resistance of the solution, a resistor R2 and capacitor C1 in parallel to model the properties of the molecular layer and double layer, and a parallel combination of resistor R3 with a constant phase element (CPE) to reflect the impedance of the anodized graphene space charge region. The CPE impedance is defined by

$$Z_{CPE} = \frac{1}{T(i\varpi)^n}$$

where T and the exponent n are nonintegral, adjustable parameters.[54] Values of $n < 1$ are often attributed to surface roughness. A CPE has to be incorporated in our model in order to adequately fit the data.

A single set of parameters was used to simultaneously fit the real and imaginary parts of the impedance over the frequency range from 0.1 Hz to 0.1 MHz. The low value of χ^2 in the order of 0.02 indicates a good fit. Table 1 gives the parameters fitted for the DNA-probe immobilized on the anodized EG electrode by covalent grafting or $\pi-\pi$ stacking, respectively, before and after hybridization with complementary or non cDNA targets.

Table 1. Results of Fitting Parameters to the Equivalent Circuit Model for DNA-Immobilization by Covalent Grafting and by $\pi-\pi$ Stacking

	C1 (μF)	R2 (kΩ)	R3 (kΩ)	T, 10^{-6}	n
			Covalent Grafting		
probe	6.19 ± 0.61	224 ± 9	267 ± 11	1.11 ± 0.02	0.87 ± 0.01
noncomplementary	6.59 ± 0.54	196 ± 7	226 ± 9	1.14 ± 0.04	0.86 ± 0.01
hybridized to target	1.84 ± 0.29	46 ± 4	443 ± 21	1.74 ± 0.05	0.82 ± 0.01
			$\pi-\pi$ Stacking		
probe	2.24 ± 0.25	94 ± 9	217 ± 29	7.74 ± 0.9	0.84 ± 0.03
noncomplementary	2.25 ± 0.25	79 ± 8	181 ± 17	7.93 ± 0.8	0.69 ± 0.02
hybridized to target	3.62 ± 0.65	45 ± 9	374 ± 9	3.77 ± 0.5	0.76 ± 0.03

From Table 1, it is noteworthy that, for both immobilizations, hybridization induced significant changes in the parameters associated with the molecular double layer, C1 and R2, and the space charge layer, R3 and T. Their values increase or decrease by more than 50% (detailed analysis in the Supporting Information). Nevertheless, DNA-hybridization presents stronger effects on anodized EG electrodes functionalized by grafted DNA-probes. This confirms the more important changes observed in the impedimetric results.

For anodized HOPG, upon hybridization, the parameters of the space charge layer and double layer increase or decrease by less than 36% (See Table 1 in the Supporting Information for detailed analysis). This further affirms that anodized EG is a better impedimetric platform for biosensing.

These results show that the space charge layer of anodized EG presents a high degree of sensitivity toward the biological environment compared to other semiconductor electrodes materials that have been used for impedimetric sensing. For p and n type silicon electrodes,[55] the modification of the space charge layer parameters are less than 3% upon full hybridization of probe and target DNA. In the case of boron doped diamond, 2% and 40% changes were measured for R3 and T, respectively.[56] In the case of EG, the changes of the space charge layer parameters, R3 and T, upon biorecognition events, are more than 50%.

Mott−Schottky Analysis. Mott−Schottky analysis is commonly used for semiconductor and film formation studies. In the Mott−Schottky analysis, the electrochemical impedance is measured over a range a potential using a single frequency. The Mott−Schottky plot represents capacitance measurements as a function of potential. The related Mott−Schottky equation is

$$\frac{1}{C_{SC}^2} = \frac{2}{\varepsilon\varepsilon_0 N}\left(E - E_{FB} - \frac{kT}{e}\right)$$

where C_{sc} = capacitance of the space charge region, ε = dielectric constant of the semiconductor, ε_0 = permittivity of free space, N = donor density (electron donor concentration for an n-type semiconductor), E = applied potential, E_{FB} = flatband potential, T = temperature, and k = Boltzmann's constant.

For a n-type semiconductor, the space-charge region is expected to be in accumulation at the most negative potentials: there is an excess of the majority charge carrier (electrons) in the space charge region. It is where the space-charge capacitance typically becomes very large (as shown Figure 2d) and $1/C_{SC}^2$ becomes correspondingly small. Since the capacitance for the anodized graphene space charge layer C_{sc} and the molecular layer capacitance C_{mol} are in series, the total capacitance of the modified surface can be represented by $C_{tot}^{-1} = C_{SC}^{-1} + C_{mol}^{-1}$. At large negative potentials, the anodized EG electrode surface is in the accumulation region, leading to a minimal $1/C_{SC}$ and the total capacitance is affected to a greater extent by the capacitance of the molecular layer. This effect complicates the analysis of the Mott−Schottky plot and would lead to inaccurate extrapolations of the flat band potentials without further correction. To generate a Mott−Schottky plot corrected for the influence of molecular capacitance, we use the limiting capacitance observed at a negative potential to extract a single value for the molecular capacitance. The space−charge capacitance is then extracted using $C_{SC}^{-1} = C_{tot}^{-1} - C_{mol}^{-1}$.

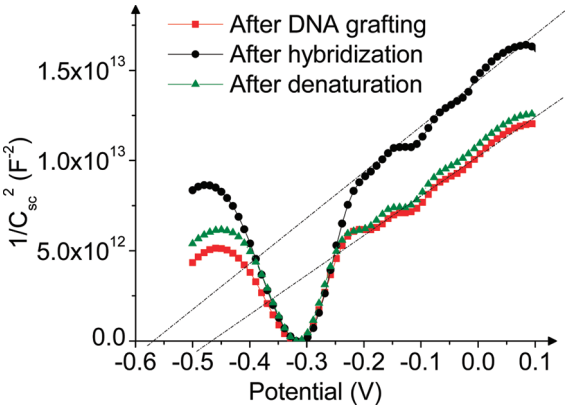

Figure 4. Mott−Schottky analysis of DNA-probe immobilized by covalent grafting onto the anodized EG surface before and after hybridization, and then after denaturation, measured at 1000 Hz.

Figure 4 shows the resulting modified Mott−Schottky plot between −0.5 and 0.1 V at 1 kHz. More positive potentials were not investigated in order to prevent the oxidation of DNA bases. The plot of $1/C_{SC}^2$ as a function of potential has the characteristic shape expected for a n-type semiconductor. $1/C_{SC}^2$ linearly decreases from 0.1 to −0.3 V, reaching a minimal value. The flat-band potential can be extracted by extrapolating $1/C_{SC}^2 = 0$ between −0.2 and 0.1 V, as $1/C_{SC}^2$ is linear over this potential range. A surface potential shift of approximately 100 mV was obtained when the DNA-targets (1 nM) were hybridized to immobilized DNA-probes. This −100 mV shift is similar in magnitude to that observed for DNA hybridization on silicon surfaces.[57] After denaturation in 0.1 M NaOH, the capacitance ($1/C_{SC}^2$) plot is almost similar to the one before hybridization, which attests to the robustness of EG as a sensing substrate.

dx.doi.org/10.1021/ac102431d |*Anal. Chem.* 2011, 83, 2452–2460

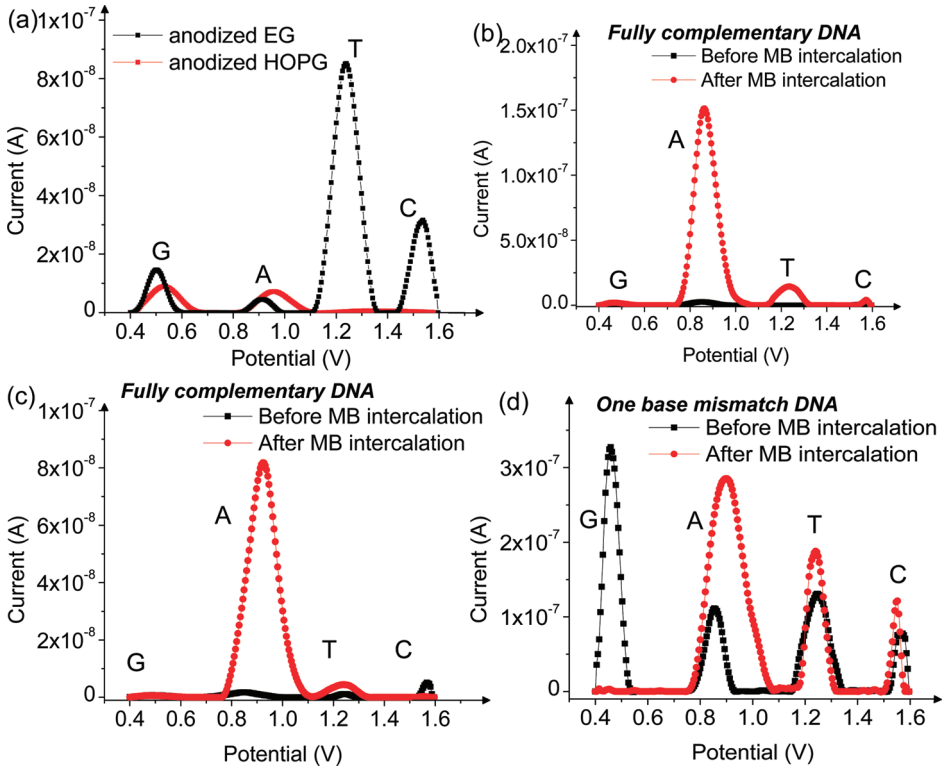

Figure 5. (a) DPV in phosphate buffer for 1 nM ssDNA solution using an anodized EG electrode (black curve) and 100 nM ssDNA solution using an anodized HOPG (red curve) electrode. DPV at the anodized EG electrode in a phosphate buffer for a (b) hybridized 1 nM probe + 1 nM target before and after MB intercalation; (c) DNA-probes immobilized by $\pi-\pi$ stacking and hybridized with 1 nM target before and after MB intercalation; (d) 1 nM probe + 1 nM target with one mismatch before and after MB intercalation.

DNA Detection by Differential Pulse Voltammetry. The direct sensing of DNA by monitoring the oxidation current of its nucleic acids can be carried out using differential pulse voltammetry (DPV). Guanine and cytosine have the lowest oxidation potential of all DNA bases, thus these bases can be more easily detected than thymine and adenine and their oxidation has been extensively studied at carbon-based electrodes.[58−62] However, the oxidation of the individual bases in DNA is much more difficult than the oxidation of free DNA bases. There have been reports of detection of bases in DNA with the help of a prehydrolysis step to release the bases into their free states.[63,64] Recently Zhou et al. reported the electrochemical oxidation of the four DNA bases in single strands DNA without pretreatment and without overlapping peaks for 9-mer ssDNA at 1 μM using chemically reduced graphene oxide.[65]

Figure 5a shows a typical differential pulse voltammogram (DPV) obtained for a solution of single stranded DNA (30-mer) at 1 nM using the EG electrode. The four well-separated peaks correspond to the oxidation of the four DNA bases: the purine bases, guanine (G) and adenine (A), and the pyrimidine bases, thymine (T) and cytosine (C). Their oxidation potentials are 0.502, 0.912, 1.238, and 1.535 V vs Ag/AgCl, respectively. These oxidation potentials are lower than those obtained with a glassy carbon electrode[66] and comparable to that obtained on a chemically reduced graphene oxide-modified glassy carbon electrode.[65]

For comparison, we have also conducted the DPV experiment on anodized HOPG. Figure 5a shows the differential pulse voltammogram obtained for a 100 nM solution of single stranded DNA on anodized HOPG electrode versus anodized EG electrode. The oxidation peaks of guanine and adenine are well-defined whereas there is no clear signal for cytosine and thymine. Moreover, the DNA oxidation peaks intensities are weaker and the peaks position shift toward a more positive potential, which reflect the difficulty to oxidize DNA on anodized HOPG as compared to anodized EG. This can be explained by the narrower electrochemical potential window and slower electron transfer kinetics on HOPG compared to EG.[34,67] Therefore, in addition to the impedimetric sensing demonstrated above, EG is also a more superior platform for DPV sensing of DNA compared to HOPG.

As shown previously by Lim et al.,[19] without the need of a prehydrolysis step, the four bases of ssDNA can be simultaneously detected by anodized EG electrodes at physiological pH. In this work, we further explored if anodized EG can be used for the direct voltammetric detection of hybridized DNA. Using EG as the electrode, we performed DPV for free DNA in solution which include single stranded DNA, hybridized DNA, as well as one-base mismatched DNA. As shown Figure 5b, the DPV of free DNA duplex in solution is characterized by weak oxidation peaks, which nevertheless proves the presence of DNA bases in solution. When the DNA duplex is formed, the DNA bases are embedded in the DNA helix structure and form hydrogen bonds with their complementary bases. Thus, for hybridized DNA fragments, the oxidation of its DNA bases is kinetically sluggish. To get a higher signal, the DNA structure can be opened by methylene blue (MB), an aromatic heterocycle that is widely used as an electrochemical intercalator to monitor the DNA hybridization reaction.[68−71] As shown in Figure 5b, the DNA oxidation peaks strongly increases after the intercalation by MB. For example, the adenine peak intensity is about 60 times higher than before MB intercalation, which proves the success of MB

intercalation in the backbone of the DNA duplex as well as the hybridization of the DNA fragments. It is noteworthy that the oxidation peaks corresponding to cytosine and guanine are smaller compared to that of the adenine peak. As the intercalation of MB in the DNA duplex occurs between guanine and cytosine,[72−76] a MB-guanine-cytosine complex could be formed preventing the oxidation of these DNA bases.

DPV was also performed on DNA which was immobilized on EG. For a $\pi-\pi$ stacked DNA duplex hybridized with cDNA-target (1 nM) on the anodized EG surface (Figure 5c), the DPV signal is around 40 times higher than before intercalation. The response is comparable to free DNA duplex in solution, confirming the successful MB intercalation in the DNA duplex and the detection of DNA hybridization. However, in the case of covalently grafted DNA-probes hybridized with DNA-target (1 nM), no significant increase in the peak intensity was observed after the addition of MB. Moreover, the guanine oxidation peak is clearly visible, which suggests that MB molecules were not intercalated in the hybridized DNA duplex. This can be explained by steric effects, and the high density of hybridized fragments prevents the intercalation of MB molecules.

Single-nucleotide polymorphisms (SNPs) are the most common type of genetic variation. A SNP is a DNA sequence variation in the genome, occurring when a single nucleotide (A, T, C, G) differs from a reference sequence. To investigate the sensing ability of anodized EG for one base mismatch, a solution containing DNA-probe (1 nM) and one single base mismatch target (1 nM) was characterized by DPV (Figure 5d). The oxidation of the free DNA fragments resulted in four intense and well-resolved peaks. Even before MB intercalation, much stronger oxidation peaks corresponding to DNA bases were obtained (about tenth of μA, Figure 5d) from the mismatched DNA as compared to that of hybridized DNA (few nA, Figure 5b), which proves that DPV is sensitive to the quality of complementary binding between probe and target. After MB intercalation, the oxidation signal slightly increases (Figure 5d): the adenine peak intensity had increased only by 2.6 times. This proves that the DNA fragments in the SNP case were not fully hybridized and consequently the MB intercalation did not produce significant improvement since most of the strands are not fully complementary. It is noted that the guanine peak is missing after MB intercalation, due to the formation of the MB-guanine complex. Our results show that it is possible to apply DPV to fully differentiate the cDNA duplex from one base mismatch target for a 30-mer DNA fragment because a strong increase in DPV signal after MB intercalation is specific to fully cDNA fragments. This method enables simple and rapid detection of DNA hybridization without the labeling and DNA immobilization step.

CONCLUSIONS

Anodized epitaxial graphene (EG) is shown to be a robust platform for label-free DNA detection by electrochemical impedance and differential pulse voltammetry. EG also presents distinct advantages over anodized graphite in terms of electrochemical sensing. Two different processes of biofuntionalization were performed: covalent grafting or $\pi-\pi$ stacking. It was found that covalent grafting of probe DNA on anodized EG affords a larger dynamic range 5×10^{-14} to 1×10^{-6} M and a more sensitive response than the $\pi-\pi$ stacked DNA probe. Equivalent circuit modeling shows that significant changes are produced in the resistance of the molecular layer and space charge layer in the EG sensor following DNA hybridization. Anodized EG also allows the direct voltammetric sensing of single-nucleotide mismatch in the DNA hybridization assay. This study demonstrates the emerging potentials of epitaxial graphene-based biosensors in sensitive and fast detection of biomolecules.

ASSOCIATED CONTENT

Supporting Information. Additional information as noted in text. This material is available free of charge via the Internet at http://pubs.acs.org.

AUTHOR INFORMATION

Corresponding Author
*E-mail: chmlohkp@nus.edu.sg.

ACKNOWLEDGMENT

K. P. Loh acknowledges the funding support of NRF-CRP Grant "Graphene Related Materials and Devices" R-143-000-360-281.

REFERENCES

(1) Novoselov, K. S.; Geim, A. K.; Morozov, S. V.; Jiang, D.; Zhang, Y.; Dubonos, S. V.; Grigorieva, I. V.; Firsov, A. A. *Science* **2004**, *306*, 666.
(2) Geim, A. K.; Novoselov, K. S. *Nat. Mater.* **2007**, *6*, 183.
(3) Stankovich, S.; Dikin, D. A.; Dommett, G. H. B.; Kohlhaas, K. M.; Zimney, E. J.; Stach, E. A.; Piner, R. D.; Nguyen, S. T.; Ruoff, R. S. *Nature* **2006**, *442*, 282.
(4) Geng, X. M.; Niu, L.; Xing, Z. Y.; Song, R. S.; Liu, G. T.; Sun, M. T.; Cheng, G. S.; Zhong, H. J.; Liu, Z. H.; Zhang, Z. J.; Sun, L. F.; Xu, H. X.; Lu, L.; Liu, L. W. *Adv. Mater.* **2010**, *22*, 638.
(5) Yoo, E.; Kim, J.; Hosono, E.; Zhou, H.; Kudo, T.; Honma, I. *Nano Lett.* **2008**, *8*, 2277.
(6) Bao, Q. L.; Zhang, H.; Yang, J. X.; Wang, S.; Tong, D. Y.; Jose, R.; Ramakrishna, S.; Lim, C. T.; Loh, K. P. *Adv. Funct. Mater.* **2010**, *20*, 782.
(7) Shan, C. S.; Yang, H. F.; Song, J. F.; Han, D. X.; Ivaska, A.; Niu, L. *Anal. Chem.* **2009**, *81*, 2378.
(8) Tan, L.; Zhou, K. G.; Zhang, Y. H.; Wang, H. X.; Wang, X. D.; Guo, Y. F.; Zhang, H. L. *Electrochem. Commun.* **2010**, *12*, 557.
(9) Wang, Q. H.; Hersam, M. C. *Nat. Chem.* **2009**, *1*, 206.
(10) Wang, X. R.; Tabakman, S. M.; Dai, H. J. *J. Am. Chem. Soc.* **2008**, *130*, 8152.
(11) Xu, Y. X.; Zhao, L.; Bai, H.; Hong, W. J.; Li, C.; Shi, G. Q. *J. Am. Chem. Soc.* **2009**, *131*, 13490.
(12) Eda, G.; Fanchini, G.; Chhowalla, M. *Nat. Nanotechnol.* **2008**, *3*, 270.
(13) Campos-Delgado, J.; Romo-Herrera, J. M.; Jia, X. T.; Cullen, D. A.; Muramatsu, H.; Kim, Y. A.; Hayashi, T.; Ren, Z. F.; Smith, D. J.; Okuno, Y.; Ohba, T.; Kanoh, H.; Kaneko, K.; Endo, M.; Terrones, H.; Dresselhaus, M. S.; Terrones, M. *Nano Lett.* **2008**, *8*, 2773.
(14) Kim, K. S.; Zhao, Y.; Jang, H.; Lee, S. Y.; Kim, J. M.; Ahn, J. H.; Kim, P.; Choi, J. Y.; Hong, B. H. *Nature* **2009**, *457*, 706.
(15) Reina, A.; Jia, X. T.; Ho, J.; Nezich, D.; Son, H. B.; Bulovic, V.; Dresselhaus, M. S.; Kong, J. *Nano Lett.* **2009**, *9*, 30.
(16) Li, X. L.; Zhang, G. Y.; Bai, X. D.; Sun, X. M.; Wang, X. R.; Wang, E.; Dai, H. J. *Nat. Nanotechnol.* **2008**, *3*, 538.
(17) Yu, A. P.; Ramesh, P.; Itkis, M. E.; Bekyarova, E.; Haddon, R. C. *J. Phys. Chem. C* **2007**, *111*, 7565.
(18) Berger, C.; Song, Z. M.; Li, X. B.; Wu, X. S.; Brown, N.; Naud, C.; Mayou, D.; Li, T. B.; Hass, J.; Marchenkov, A. N.; Conrad, E. H.; First, P. N.; de Heer, W. A. *Science* **2006**, *312*, 1191.
(19) Lim, C. X.; Hoh, H. Y.; Ang, P. K.; Loh, K. P. *Anal. Chem.* **2010**, *82*, 7387.

(20) Moulton, S. E.; Barisci, J. N.; Bath, A.; Stella, R.; Wallace, G. G. *Langmuir* **2005**, *21*, 316.
(21) Lasseter, T. L.; Cai, W.; Hamers, R. J. *Analyst* **2004**, *129*, 3.
(22) Smiechowski, M. F.; Lvovich, V. F.; Roy, S.; Fleischman, A.; Fissell, W. H.; Riga, A. T. *Biosens. Bioelectron.* **2006**, *22*, 670.
(23) Tlili, C.; Korri-Youssoufi, H.; Ponsonnet, L.; Martelet, C.; Jaffrezic-Renault, N. J. *Talanta* **2005**, *68*, 131.
(24) Chen, C. P.; Ganguly, A.; Wang, C. H.; Hsu, C. W.; Chattopadhyay, S.; Hsu, Y. K.; Chang, Y. C.; Chen, K. H.; Chen, L. C. *Anal. Chem.* **2009**, *81*, 36.
(25) Zebda, A.; Labeau, M.; Diard, J. P.; Lavalley, V.; Stambouli, V. *Sens. Actuators, B: Chem.* **2010**, *144*, 176.
(26) Hiromoto, S.; Noda, K.; Hanawa, T. *Corros. Sci.* **2002**, *44*, 955.
(27) Kan, E. J.; Li, Z. Y.; Yang, J. L.; Hou, J. G. *J. Am. Chem. Soc.* **2008**, *130*, 4224.
(28) Rudberg, E.; Salek, P.; Luo, Y. *Nano Lett.* **2007**, *7*, 2211.
(29) Sharma, R.; Nair, N.; Strano, M. S. *J. Phys. Chem. C* **2009**, *113*, 14771.
(30) Son, Y. W.; Cohen, M. L.; Louie, S. G. *Phys. Rev. Lett.* **2006**, *97*, 216803.
(31) Davies, T. J.; Hyde, M. E.; Compton, R. G. *Angew. Chem., Int. Ed.* **2005**, *44*, 5121.
(32) Rice, R. J.; McCreery, R. L. *Anal. Chem.* **1989**, *61*, 1637.
(33) Bowling, R.; Packard, R. T.; McCreery, R. L. *Langmuir* **1989**, *5*, 683.
(34) Jia, J. B.; Kato, D.; Kurita, R.; Sato, Y.; Maruyama, K.; Suzuki, K.; Hirono, S.; Ando, T.; Niwa, O. *Anal. Chem.* **2007**, *79*, 98.
(35) Dreyer, D. R.; Park, S.; Bielawski, C. W.; Ruoff, R. S. *Chem. Soc. Rev.* **2010**, *39*, 228.
(36) Loh, K. P.; Bao, Q. L.; Ang, P. K.; Yang, J. X. *J. Mater. Chem.* **2010**, *20*, 2277.
(37) Cole, K. S.; Cole, R. H. *J. Chem. Phys.* **1941**, *9*, 341.
(38) Soon, J. M.; Loh, K. P. *Electrochem. Solid-State Lett.* **2007**, *10*, A250.
(39) Kelley, S. O.; Barton, J. K. *Science* **1999**, *283*, 375.
(40) Kelley, S. O.; Jackson, N. M.; Hill, M. G.; Barton, J. K. *Angew. Chem., Int. Ed.* **1999**, *38*, 941.
(41) Schuster, G. B. *Acc. Chem. Res.* **2000**, *33*, 253.
(42) Baur, J.; Gondran, C.; Holzinger, M.; Defrancq, E.; Perrot, H.; Cosnier, S. *Anal. Chem.* **2010**, *82*, 1066.
(43) Vagin, M. Y.; Trashin, S. A.; Karyakin, A. A.; Mascini, M. *Anal. Chem.* **2008**, *80*, 1336.
(44) Jenkins, D. M.; Chami, B.; Kreuzer, M.; Presting, G.; Alvarez, A. M.; Liaw, B. Y. *Anal. Chem.* **2006**, *78*, 2314.
(45) Kjallman, T. H. M.; Peng, H.; Soeller, C.; Travas-Sejdic, J. *Analyst* **2010**, *135*, 488.
(46) Bonanni, A.; Pumera, M.; Miyahara, Y. *Anal. Chem.* **2010**, *82*, 3772.
(47) Tang, L. A. L.; Wang, J. Z.; Loh, K. P. *J. Am. Chem. Soc.* **2010**, *132*, 10976.
(48) Goh, M. S.; Pumera, M. *Electrochem. Commun.* **2010**, *12*, 1375.
(49) Bonanni, A.; Pividori, M. I.; del Valle, M. *Anal. Bioanal. Chem.* **2007**, *389*, 851.
(50) Yang, N.; Uetsuka, H.; Osawa, E.; Nebel, C. E. *Angew. Chem., Int. Ed.* **2008**, *47*, 5183.
(51) Wang, J.; Li, S. P.; Zhang, Y. Z. *Electrochim. Acta* **2010**, *55*, 4436.
(52) Xu, Y.; Ye, X. Y.; Yang, L.; He, P. A.; Fang, Y. Z. *Electroanalysis* **2006**, *18*, 1471.
(53) Dong, X. C.; Shi, Y. M.; Huang, W.; Chen, P.; Li, L. J. *Adv. Mater.* **2010**, *22*, 1649.
(54) Macdonald, J. R. *Solid State Ionics* **1984**, *13*, 147.
(55) Cai, W.; Peck, J. R.; van der Weide, D. W.; Hamers, R. J. *Biosens. Bioelectron.* **2004**, *19*, 1013.
(56) Yang, W. S.; Butler, J. E.; Russell, J. N.; Hamers, R. J. *Langmuir* **2004**, *20*, 6778.
(57) Cloarec, J. P.; Deligianis, N.; Martin, J. R.; Lawrence, I.; Souteyrand, E.; Polychronakos, C.; Lawrence, M. F. *Biosens. Bioelectron.* **2002**, *17*, 405.
(58) Abbaspour, A.; Noori, A. *Analyst* **2008**, *133*, 1664.
(59) Oliveira-Brett, A. M.; Diculescu, V.; Piedade, J. A. P. *Bioelectrochemistry* **2002**, *55*, 61.
(60) Sun, W.; Li, Y. Z.; Duan, Y. Y.; Jiao, K. *Biosens. Bioelectron.* **2008**, *24*, 988.
(61) Wu, K. B.; Fei, J. J.; Bai, W.; Hu, S. S. *Anal. Bioanal. Chem.* **2003**, *376*, 205.
(62) Zari, N.; Mohammedi, H.; Amine, A.; Ennaji, M. M. *Anal. Lett.* **2007**, *40*, 1698.
(63) Zhang, R. Y.; Wang, X. M.; Chen, C. *Electroanalysis* **2007**, *19*, 1623.
(64) Abdullin, T. I.; Nikitina, I. I.; Ishmukhametova, D. G.; Budnikov, G. K.; Konovalova, O. A.; Salakhov, M. K. *J. Anal. Chem.* **2007**, *62*, 599.
(65) Zhou, M.; Zhai, Y. M.; Dong, S. J. *Anal. Chem.* **2009**, *81*, 5603.
(66) Oliveira-Brett, A. M.; Piedade, J. A. P.; Silva, L. A.; Diculescu, V. C. *Anal. Biochem.* **2004**, *332*, 321.
(67) Niwa, O.; Jia, J.; Sato, Y.; Kato, D.; Kurita, R.; Maruyama, K.; Suzuki, K.; Hirono, S. *J. Am. Chem. Soc.* **2006**, *128*, 7144.
(68) Arias, P.; Ferreyra, N. F.; Rivas, G. A.; Bollo, S. *J. Electroanal. Chem.* **2009**, *634*, 123.
(69) Kara, P.; Kerman, K.; Ozkan, D.; Meric, B.; Erdem, A.; Ozkan, Z.; Ozsoz, M. *Electrochem. Commun.* **2002**, *4*, 705.
(70) Kelley, S. O.; Barton, J. K.; Jackson, N. M.; Hill, M. G. *Bioconjugate Chem.* **1997**, *8*, 31.
(71) Teh, H. F.; Gong, H. Q.; Dong, X. D.; Zeng, X. T.; Tan, A. L. K.; Yang, X. H.; Tan, S. N. *Anal. Chim. Acta* **2005**, *551*, 23.
(72) Enescu, M.; Levy, B.; Gheorghe, V. *J. Phys. Chem. B* **2000**, *104*, 1073.
(73) Farjami, E.; Clima, L.; Gothelf, K. V.; Ferapontova, E. E. *Analyst* **2010**, *135*, 1443.
(74) Hossain, M.; Kumar, G. S. *Mol. Biosyst.* **2009**, *5*, 1311.
(75) Rohs, R.; Sklenar, H.; Lavery, R.; Roder, B. *J. Am. Chem. Soc.* **2000**, *122*, 2860.
(76) Tuite, E.; Norden, B. *J. Am. Chem. Soc.* **1994**, *116*, 7548.